Human tooth enamel tuft drapes revealed by microtomography

Alban Desoutter, Ivan Panayotov, Frédéric Cuisinier, Delphine Carayon

Human tooth enamel tuft drapes revealed by microtomography

A. Desoutter [a,*], I. Panayotov [a,b,c], F. Cuisinier [a,b,c], D. Carayon [a,b,c]

[a] LBN, Univ. Montpellier, 545 Avenue Professeur Jean-Louis Viala, 34193 Montpellier Cedex 5, France
[b] UFR Odontologie, Univ. Montpellier, Montpellier, France
[c] CSERD, CHU Montpellier, Montpellier, France

Keywords:
Tooth
Dental enamel
X-ray microtomography

A B S T R A C T

Objective: The tufts of human dental enamel are structures located at the enamel-dentin junction and whose origin has not been clearly established. Although studies have highlighted their protein content and hypomineralization, none has been able to shed light on their 3D structure. The aim of this study was to reveal the whole structure using high-resolution conventional microtomography.
Design: Ten adult mandibular first and second molars and two primary mandibular first molars were sectioned and scanned with microcomputed tomography with a resolution between 4.7 and 5 micrometers. By determining the threshold discriminating dentin and tufts, we were able to reconstruct 3D meshes.
Results: We revealed the exact pattern of the tufts in adult molars and discovered their distribution, their dynamics, and the existence of a regular undulation, forming a particular angle of approximately 30 degrees with the dentin surface. A spatial frequency of approximately 160 micrometers would be compatible with the variation in the orientation of groups of dental enamel rods. In contrast, the present setting is not sufficient to extract similar information for primary teeth.
Conclusions: Enamel tufts have a specific pattern, with an oriented draped form and are regularly spaced. The possible connection between these undulations and the Hunter-Schreger bands (diazonias and parazonias) needs to be studied.

1. Introduction

Dental enamel is the "hardest" tissue of the human body, with a Young's modulus between 70 and 100 GPa, depending on the type (incisor, molar, canine…), age and teeth (Habelitz et al., 2001a; Xu et al., 1998; Zheng et al., 2013). The enamel structure consists primarily of calcium hydroxyapatite (96 wt%), protein (2 wt%) and water. Under the enamel layer, dentin is a mineralized connective structure comprised of 45% hydroxyapatite, 33% organic material and 22% water. The dentin organic phase is primarily type I collagen (90%), with a low percentage of type III, V, and fibronectin, and 10% water-rich non-collagenous proteins (proteoglycans and glycosaminoglycans) (Ten Cate & Nanci, 2013). At the interface of the enamel and dentin, four features have been described: tubular dentin, mantle dentin, and aprismatic and prismatic enamel. This transitional zone **is** called the dentin-enamel junction (DEJ). The enamel rods are not colinear and form angles between each other (Beniash et al., 2019). The result of this structure is incredibly resilient during the tooth's life. Each day, thousands of times, teeth are subjected to forces during eating that can reach 1000 N, with a mean of approximately 700 N, depending on sex, age, weight, and pathology (Braun et al., 1995). Enamel is very hard, but as a nonductile material, it is fragile. The fracture toughness of external and internal enamel were established in controlled crack growth experiments as 0.67 $\pm$0.12 MPa·m$^{0.5}$ and 1.13–3.93 MPa·m$^{0.5}$, respectively. Tufts are the primary fracture sources, but prism interweaving and self-healing could limit crack propagation (Bajaj & Arola, 2009).

The secondary structures of enamel in the vicinity of the DEJ are tufts, lamellae and spindles (Palamara et al., 1989). Tufts are linked to orientation changes in ameloblasts. The resulting divergence of enamel rods creates hypomineralized spaces starting in the DEJ. Tufts must not be confused with lamellae, which is a linear defect starting at DEJ and proceeding through the enamel to the surface (Palamara et al., 1989). The lamella, spindle and tuft are hypomineralized formations, with different ratios of phosphate and calcium (Ogita et al., 1998). Tufts are classically described as hypomineralized ribbon-like structures (Fig. 1) starting at the DEJ and extending to a inner third of the thickness of the

* Corresponding author.
E-mail addresses: alban.desoutter@umontpellier.fr (A. Desoutter), ivan.panayotov@umontpellier.fr (I. Panayotov), frederic.cuisinier@umontpellier.fr (F. Cuisinier), delphine.carayon@umontpellier.fr (D. Carayon).

enamel. The 3D shape of the tuft has been analysed by optical microscopy by changing the focal plane every 6 µm. Tufts appeared as undulating, disorganized structures (Osborn, 1969). These structures were also observed in bovine teeth (Mehr et al., 2012).

A combined scanning and transmission electron microscopy examination of etched human teeth defined tufts as having "*a wavy course and appearing as bundles of tubular structures*". (Amizuka et al., 1992). Enamel tufts exhibit a relatively simple ordering in rows away from the cusp. Since tufts lie between prisms, they indicate disorder in the patterning of ameloblast trajectories at the dentin surface. Strain-cued motility was proposed to explain the formation of dental enamel structures, mainly curved prisms. Dental enamel is formed during amelogenesis by a population of ameloblasts that move about laterally within an expanding curved sheet, subject to continuously evolving spatial and temporal gradients in the strain (Cox & Snead, 2016). Such theories give little explanation of the tufts' presence on the surface of the dentin. One of their functions could be to limit the strain between or inside ameloblast groups. Tufts at the interface of dentin and enamel, containing organic matter, could stabilize the tooth against the propagation of a break by self-healing (Myoung et al., 2009). The tufts would therefore play the role of preventing cracks but initiate them when there is too much stress at one point. Confocal Raman microscopy revealed that the tuft width ranges from 5 to 15 µm, and the height can reach 150/200 µm: the phosphate peak intensity (PO_4^{3-}) decreases between 6 and 8 times (Desoutter et al., 2021).

As the 3D organization of tufts remains elusive with no direct 3D observation since the primary paper of Amizuka et al. (Amizuka et al., 1992), we aimed to use high-resolution µCT with a large field of view. An entire tooth, or a large portion of it, can be scanned with 4.5 to 5 micrometer resolution superior to the tuft width ranging from 5 to 10 µm.

2. Materials and methods

2.1. Sample preparation

Ten human first and second mandibular molar teeth (5 each), extracted for orthodontic reasons with patient consent - process No. 2014–2198 - local ethical research committee "Montpellier Sud-Méditerranée IV", were collected and stored in distilled water. All donors were Europeans between 25 and 40 years old; 6 teeth were from men and 4 from women. Each tooth was sectioned to create a 3x3x3 mm^3 specimen, including the cusp, enamel and dentin. The cube-shaped samples were preserved in distilled water. To compare with the results obtained with adult teeth, two deciduous molars were also prepared.

2.2. Microtomography

Each sample was placed in an EasyTom 150 kV microcomputed tomography with an Xact software interface (RX Solution, Chavanod, France). A 1 mm aluminum filter was placed in front of the X-ray source. The voltage used was 71 kV, with an intensity of 66 µA and a tube power of 4.68 W. To increase the signal-to-noise ratio (SNR), 4 images were recorded and averaged, and the gain reached 7, with an angular step of 0.25 degrees. A total of 1440 radiography-type images were collected over approximately 30 minutes, and the reconstruction algorithm was performed by Xact software. A total of 1808 16-bit Tiff images were reconstructed in gray shades image, with a voxel size in the range of 4.7 to 5 micrometers. Ring artefacts and beam hardening corrections were not used.

2.3. Calculation of density

The reconstructed greyscale intensity of each image voxel does not relate directly to mineral density alone. We assume that the X-ray attenuation within enamel is dominated by and can be approximated as the X-ray attenuation of the mineral compound hydroxyapatite (HA), which has the formula $Ca_5(PO_4)_3(OH)$. Assuming a density of 2.72 g/cm^3 for enamel and 1.97 g/cm^3 for dentin (Gradl et al., 2016), we evaluated the variation in density in the tuft with a linear relationship between those two values and their gray shade.

2.4. Surface reconstruction

Tuft intensity profiles were performed with FIJI (v1.53c, National Institutes of Health, USA) and exported in Excel to be plotted. This allowed measurement of the width of the tufts.

To visualize the tuft structure in 3D, gray shade images were imported into FIJI and transformed into binary images to select the voxels of interest.

To select the pixels of interest, the gray level values and standard deviations of the dentin, enamel and tuft centers were retrieved. For dentin, the mean value minus two standard deviation values was taken. To select the pixels of the tufts, an empirical method was used: the upper threshold was taken as the mean value minus three standard deviations.

Gaussian low-pass filtering smoothing was applied with sigma (standard deviation) equal to 1. The surface was visualized in FIJI (3D viewer) and exported as an STL file. Resampling and cropping of the ROI was performed in MeshLab (v2020.12, Consiglio Nazionale delle Ricerche, Italy).

2.5. Results

Tufts appear as clear ribbon-like structures perpendicular to the DEJ

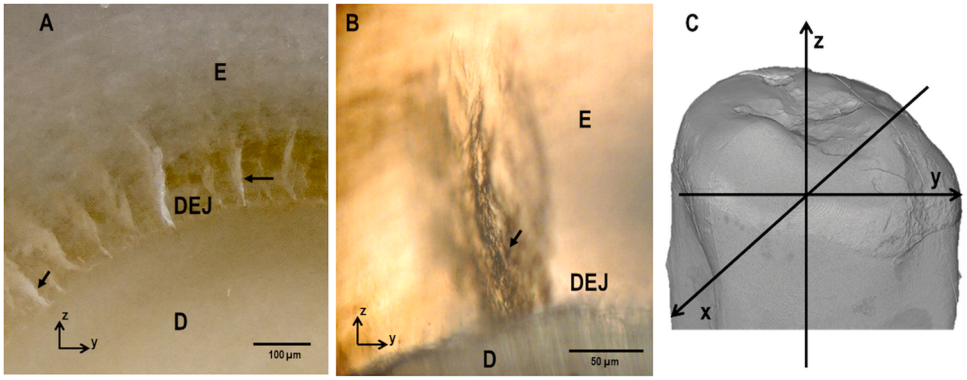

Fig. 1. A-B) Optical microscopy image of a first mandibular molar tooth at the enamel dentin junction area. D: dentin, E: enamel; DEJ: dentin enamel junction; black arrows: tufts. C) Molar surface and geometrical axis used in the present study.

and expand in the enamel (Fig. 1). In all figures presented in this article, the x-y plane is tangential to the DEJ, the x-axis is perpendicular to it, and the z-axis is colinear to the longitudinal tooth axis (see Fig. 1C).

For each sample scanned by μCT, 1808 gray shade images were obtained, and approximately 1600 image stacks were finally selected after cropping. On each sample, we can distinguish a series of white pixels forming a wave-shaped structure starting at DEJ and penetrating the enamel to a 200 μm depth (Fig. 2A, C). When observed along the x-axis, the tufts appear as continuous wavy hypomineralized lines. The tuft lines are collinear (Fig. 2B).

Reconstructed 3D meshes allow visualization of the tuft lines. They confirm that the longitudinal axis of the lines and their wavy shape surface extracted after thresholding permits visualization of the distribution of the tufts and orientation of the wave pattern. See Fig. 3. The surface of interest, where the tufts are clearly visible with a pattern, extends to a length of 2.5 mm.

Microtomography images and 3D meshes allow accurately measurement of the morphology of the tufts.

All measures obtained from 40 tuft drapes are presented in Table 1. In this table, the maximum height is the maximum distance between the DEJ and the top of the tuft. The tuft drapes length is from the cusp to the apical ends. The tuft width is measured in several zones of the tuft. The space between the tufts represents the distance between two tufts draped along the y-axis; the drape spatial periodicity is measured as the distance between two undulation ridges; the α angle, as shown in Fig. 4A, is the angle between the drape ridge and the DEJ; and finally the tuft gray value converted to grams/cmˆ3 of HA.

The results obtained for primary teeth did not allow us to clearly highlight the 3D structure of the tufts.

3. Discussion

To our knowledge, the 3D structure of tufts has never been described. Tufts are almost always described as 2-dimensional structures, classified as enamel secondary structures, ranging from the DEJ to the first third of the enamel thickness. The micro-CT revealed that the 2D structures correspond to 3D drapes extending longitudinally from the cusp area in the direction of the tooth collar, spreading over 2.5 mm.

Amizuka et al. in 1992 described tuft and tuft plates that could be related to tuft drapes. On scanning electron microscopy images of dentin surface, after the enamel has been removed by etching, tufts cover the perimeter of the premolar very homogeneously. This divergence in

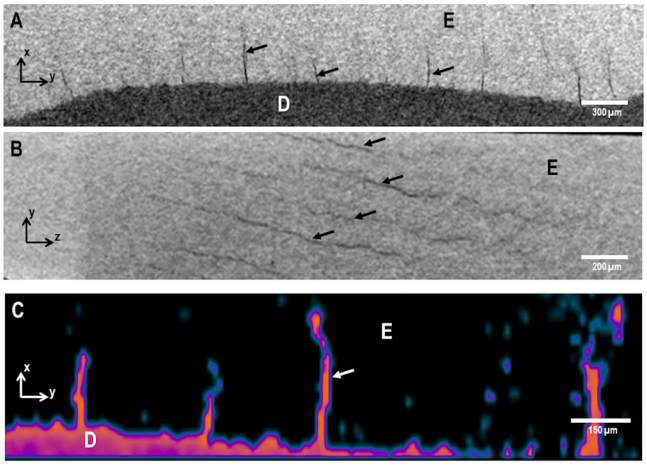

Fig. 2. Permanent molar A) microtomography gray shade image in a plane perpendicular to the DEJ. Arrows: tufts B) microtomography gray shade image view along the x-axis perpendicular to the DEJ, i.e., perpendicular to picture A; tufts appear as wavy black lines (indicated by arrows); C) microtomography image of tufts after data treatments by interpolation and Laplacian smoothing; same orientation as image A.

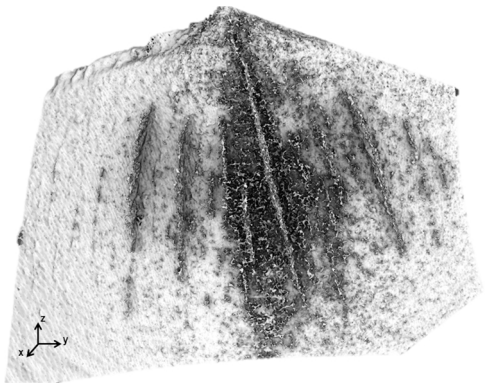

Fig. 3. 3D mesh reconstruction of a large field of view of DEJ with tuft.

Table 1
Tufts drapes morphological parameters. Angulation α: angle between the dentin and orientation of the wave-shaped pattern (see Fig. 4); n (tufts): 40.

	Units	Mean	Range of value
Maximum height (x axis)	μm	207	194–220
length	μm	1003	906–1100
width	μm	15	12–18
distance between drapes	μm	188	153–223
spatial periodicity	μm	163	146–180
α angle	degree	31	29–33
tuft density	g/cm3	2.15	2.08–2.22

results could be explained by the teeth type or by the population studied. Comparatively, we provided actual 3D images of tufts drapes, and we also determined the degree of mineralization of these structures, without having to remove the enamel, in a totally nondestructive way. The structure of these tufts clearly indicates a particular pattern found in all the samples: an undulation, with a clearly marked periodicity. See Fig. 4 in particular.

The enamel prisms have a diameter of approximately 5 μm (Habelitz et al., 2001b), so the undulation observed cannot be the result of a variation in the orientation of single prisms. It is more likely that these hypomineralized structures are the result of a variation in the orientation of ameloblast clusters during the hydroxyapatite mineralization phase. The characteristic distance between two tufts is 188 μm (SD 71), and the average of the spatial periods observed for the tuft corrugations is 163 μm (SD 34). Hunter-Schreger bands have spatial periods that range from 83 to 250 μm for permanent molars enamel (Lynch et al., 2010). The range of such values is concordant with the periodicity observed. It is therefore possible that the undulation of the tufts can be correlated with the formation of Hunter-Schreger bands. However, angulation of such bands and DEJ in molars is approximately 35/40 degrees, more than the angulation of the tuft wave pattern reported in Table 1. The angulation of the tufts drapes undulation could be related to the orientation of the trajectory of the ameloblast populations relative to the growth front (Cox & Snead, 2016).

Amelogenesis starts at the dentine surface at the cuspal tip of the mesenchymal papilla. The strain-cued model of ameloblast migration is based on a homogeneous and continuous layer of cells perpendicular to the growth front (Cox & Snead, 2016). The layer of ameloblasts is relatively rigid, as the cell bodies are elongated, and two junctional complexes associated with terminal webs are present at both extremities. If the curvature of the growth front exceeds the elasticity of the ameloblast layer, a local defect could appear. These defects, as grain boundaries in the material, could migrate and form dislocations. Dislocation locally accumulates in the constraint, and this is possibly the role of the tufts drapes.

Regarding the content of the structure itself, the results here must be interpreted with great caution. Indeed, the tufts are hypomineralized,

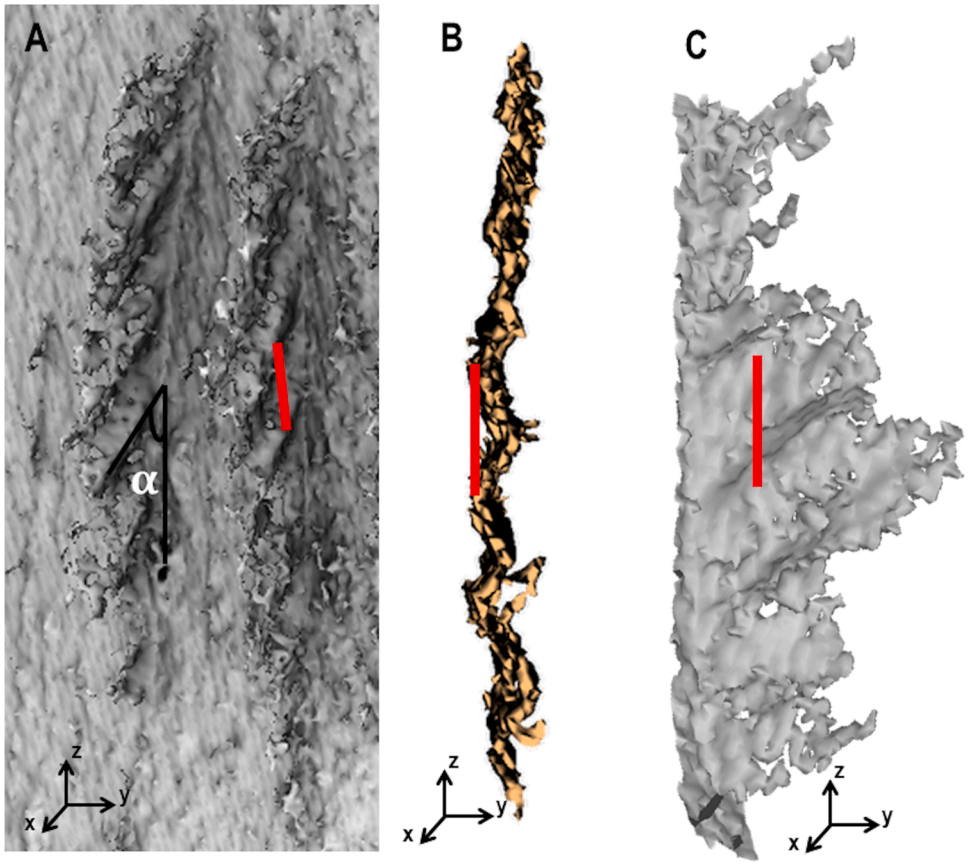

Fig. 4. A, B, C) Three different views of a tuft line. A: α: angle between the dentin surface (y,z plane) and the ridge of the wave-shaped tufts (black line). A and B are figures extracted from mesh seen in Fig. 3; Red line: spatial periodicity of waves. (For interpretation of the references to color in this figure legend, the reader is referred to the web version of this article.)

and the values found in this study are 2.15 g/cm^3, i.e., a density between dentin and enamel. Due to the characteristic size of a tuft, we could not draw conclusions about the content of the tuft, i.e., whether it is a weakly mineralized structure, containing more organic matter, or whether it is a space totally devoid of any mineral phase. This question highlights a limitation of the present study: the resolution reveals the 3D structure of the enamel tufts but does not allow us to know its interior architecture. Additionally, it is possible that existing structures smaller than the resolution or of the same size were missed. A future study combining a resolution close to or below a micrometer and a large field of view will be required to examine the whole sample.

Concerning the primary teeth, 3D structures are also visible. Moreover, the undulation with spatial periodicity seems to be similar to that of adult teeth. However, the width and/or the degree of mineralization make the SNR very weak and does not permit visualization of the whole region of interest with tufts. See Supplementary Fig. 2. This did not allow for studying the 3D structure. Finally, some lines of draped tufts are visible, but only for a few hundred micrometers. With our settings, conventional microtomography, even with a high resolution, does not permit the study of tufts in primary teeth to extract morphological parameters.

4. Conclusion

Microtomography, with its voxel size below 5 µm and a field of view **in** the order of approximately 20 millimeters, makes it possible to reconstruct the 3D secondary structures of the enamel. We thus noticed that the tufts of the enamel, in permanent molars, form wavy drapes starting from the cusp in the direction of the collar, of a total length that can exceed a millimeter, and of a height that can reach more than 200 micrometers. The drapes have a periodic undulation of approximately 160 micrometers, forming an inclination with the surface of the dentin of approximately thirty degrees. This hypomineralized structure could therefore be related to a variation in the orientation of the enamel prism groups. These elements make it possible to consider a comparison with the enamel dentin junction in different human populations and to verify their presence within the animal kingdom. Finally, more powerful tools, such as a synchrotron X-ray source, with increased resolution and still a wide field of view, would be able to give further details about the architecture of the secondary structures of the DEJ. This is also necessary to improve the image quality, in particular the SNR, and extract information from primary teeth.

CRediT authorship contribution statement

A. Desoutter: contributed to conception and design, data acquisition, analysis, and interpretation, drafted and critically revised manuscript. **I. Panayotov:** contributed to analysis, drafted manuscript and critically revised manuscript. **F. Cuisinier:** contributed to conception and design, data interpretation, drafted manuscript, critically revised manuscript. **D. Carayon:** contributed to conception and design, data interpretation, drafted manuscript, critically revised manuscript.

Declaration of Competing Interest

The authors declare that they have no known competing financial interests or personal relationships that could have appeared to influence the work reported in this paper.

Acknowledgments

Authors thank Renaud Lebrun for his assistance in data acquisition. 3D data acquisitions were performed using the μ-CT facilities of the MRI platform member of the national infrastructure France-BioImaging supported by the French National Research Agency (ANR-10-INBS-04, «Investments for the future»), and of the Labex CEMEB (ANR-10-LABX-0004) and NUMEV (ANR-10-LABX-0020).

The authors would like to thank Paul Tafforeau, Beamline scientist in Structure of Material group at Synchrotron (Grenoble) and specialist of tooth enamel, for his comment on images and discussion about enamel tufts.

This research was not funded by any state or institutional agency.

Appendix A. Supplementary material

Supplementary data associated with this article can be found in the online version at doi:10.1016/j.archoralbio.2022.105487.

References

Amizuka, N., Uchida, T., Fukae, M., Yamada, M., & Ozawa, H. (1992). Ultrastructural and immunocytochemical studies of enamel tufts in human permanent teeth. *Archives of Histology and Cytology, 55*(2), 179–190.

Bajaj, D., & Arola, D. D. (2009). On the R-curve behavior of human tooth enamel. *Biomaterials, 30*(23), 4037–4046.

Beniash, E., Stifler, C. A., Sun, C.-Y., Jung, G. S., Qin, Z., Buehler, M. J., & Gilbert, P. U. P. A. (2019). The hidden structure of human enamel. *Nature Communications, 10*(1), 4383. https://doi.org/10.1038/s41467-019-12185-7

Braun, S., Bantleon, H.-P., Hnat, W. P., Freudenthaler, J. W., Marcotte, M. R., & Johnson, B. E. (1995). A study of bite force, part 1: Relationship to various physical characteristics. *The Angle Orthodontist, 65*(5), 367–372.

Cox, B. N., & Snead, M. L. (2016). Cells as strain-cued automata. *Journal of the Mechanics and Physics of Solids, 87*, 177–226.

Desoutter, A., Slimani, A., Tassery, H., Cuisinier, F., Sauro, S., Salehi, H., & Panayotov, I. (2021). Confocal Raman data analysis of tufts and spindles at the human dentin-enamel junction. *Archives of Oral Biology, 131*, Article 105262.

Habelitz, S., Marshall, S. J., Marshall, G. W., Jr, & Balooch, M. (2001a). Mechanical properties of human dental enamel on the nanometre scale. *Archives of Oral Biology, 46*(2), 173–183.

Habelitz, S., Marshall, S. J., Marshall, G. W., Jr, & Balooch, M. (2001b). Mechanical properties of human dental enamel on the nanometre scale. *Archives of Oral Biology, 46*(2), 173–183.

Lynch, C. D., O'Sullivan, V. R., Dockery, P., McGillycuddy, C. T., & Sloan, A. J. (2010). Hunter-Schreger band patterns in human tooth enamel. *Journal of Anatomy, 217*(2), 106–115.

Mehr, K., Piotrowski, P., Frączak, B., & Matthews-Kozanecka, M. (2012). Histomorphometric evaluation of organic enamel elements in erupted bovine teeth. Part I. Enamel tufts. *Bulletin of the Veterinary Institute in Pulawy*, 56. https://doi.org/10.2478/v10213-012-0121-2

Myoung, S., Lee, J., Constantino, P., Lucas, P., Chai, H., & Lawn, B. (2009). Morphology and fracture of enamel. *Journal of Biomechanics, 42*(12), 1947–1951.

Ogita, Y., Iwai-Liao, Y., & Higashi, Y. (1998). A histological study of the organic elements in the human enamel focusing on the extent of the odontoblast process. *Okajimas Folia Anatomica Japonica, 74*(6), 317–327.

Osborn, J. W. (1969). The 3-dimensional morphology of the tufts in human enamel. *Cells Tissues Organs, 73*(4), 481–495.

Palamara, J., Phakey, P. P., Rachinger, W. A., & Orams, H. J. (1989). The ultrastructure of spindles and tufts in human dental enamel. *Advances in Dental Research, 3*(2), 249–257.

Ten Cate, A. R., & Nanci, A. (2013). *Ten Cate's oral histology: Development, structure, and function*. Elsevier.

Xu, H. H. K., Smith, D. T., Jahanmir, S., Romberg, E., Kelly, J. R., Thompson, V. P., & Rekow, E. D. (1998). Indentation damage and mechanical properties of human enamel and dentin. *Journal of Dental Research, 77*(3), 472–480.

Zheng, Q., Xu, H., Song, F., Zhang, L., Zhou, X., Shao, Y., & Huang, D. (2013). Spatial distribution of the human enamel fracture toughness with aging. *Journal of the Mechanical Behavior of Biomedical Materials, 26*, 148–154.